

# ACCESSING HIGHLY OUT-OF-ECLIPTIC SCIENCE ORBITS VIA LOW-ENERGY, LOW-THRUST TRANSPORT MECHANISMS

Jeffrey Stuart\*, Rodney L. Anderson\*, Christopher Sullivan<sup>†</sup>, and Natasha Bosanac<sup>†</sup>

Several mission concepts entail the placement of a spacecraft into a high inclination orbit with respect to the ecliptic plane. Among these mission concepts are solar observatories targeting the polar regions of the Sun or spacecraft seeking an external vantage point on the zodiacal dust cloud of our solar system. In this investigation, techniques for low-thrust and low-energy trajectory design will be integrated into a cohesive framework to access these highly out-of-ecliptic science orbits. The focus of this investigation will be on spacecraft conforming to a SmallSat form-factor, enabling opportunistic science as secondary payloads or via smaller launch vehicles.

## INTRODUCTION

Trajectories that deliver spacecraft well above and below the solar system ecliptic plane are enabling for a variety of mission concepts in heliophysics and astronomy. Excursions of even  $15^\circ$  would enable observers an external view of the 3D structure of the zodiacal dust cloud, with implications for solar system evolution and exoplanetary surveys.<sup>1,2</sup> Furthermore, out-of-ecliptic trajectories offer a line-of-sight to the poles of the Sun: regions not investigated in depth since the Ulysses mission.<sup>3-5</sup> However, the Ulysses mission required a flyby of Jupiter to access an orbital inclination of nearly  $80^\circ$ , a factor that drove many other elements of the mission architecture. In contrast, current electric propulsion systems are capable of delivering a high total impulse to a spacecraft, albeit over a long period of engine operation, potentially opening avenues for alternate mission architectures. In particular, spacecraft tailored to a CubeSat or SmallSat form factor<sup>6</sup> may be launched as secondary payloads and then guided to access a variety of target science orbits,<sup>7-9</sup> greatly widening the scope for mission concept development. Furthermore, recently developed small launch vehicles provide affordable access to space for CubeSat and SmallSat missions. Thus, the focus of this investigation is leveraging high-efficiency, low-thrust propulsion on SmallSat platforms to enable missions to science orbits with significant out-of-ecliptic excursions.

Propellant-optimal, low-thrust trajectories realized by constant specific impulse (CSI) systems in nonlinear dynamical regimes typically require coasting arcs and the careful balancing of engine capability with transfer time. Therefore, a variable specific impulse (VSI) engine that varies the optimal thrust magnitude is selected to simplify the generation of transfer solutions.<sup>10</sup> Accordingly, no coasting arcs are required for the orbit transfer and the initial generation of optimal trajectories is less restrictive than an equivalent CSI transfer in terms of thrust duration. Examples of VSI engines

---

\*Mission Design & Navigation, NASA Jet Propulsion Laboratory, California Institute of Technology

<sup>†</sup>Smead Department of Aerospace Engineering Sciences, University of Colorado Boulder

currently in development include the Variable Specific Impulse Magnetoplasma Rocket (VASIMR) currently under development by the Ad Astra Rocket Company<sup>11</sup> and the Electron and Ion Cyclotron Resonance (EICR) Plasma Propulsion Systems at Kyushu University in Japan.<sup>12</sup> Though a VSI engine model is employed to generate preliminary trajectories, specific trajectories of interest can be transitioned to models incorporating higher fidelity current- and near-term engine models. For example, high specific impulse portions of the VSI thrust arcs may be replaced by coast arcs for corresponding CSI systems and spacecraft and mission parameters may be adjusted to better reflect current propulsion capabilities.<sup>13</sup>

The use of low-energy trajectories in combination with low-thrust propulsion systems has the potential to improve the generation of these optimized trajectories or produce new mission-enabling solutions. Early observations of the solutions obtained using the Mystic optimization software<sup>14–16</sup> were found to heuristically follow the invariant manifolds of unstable periodic orbits in the Circular Restricted Three-Body Problem (CR3BP).<sup>17</sup> Anderson and Lo also demonstrated that the optimized trajectories for tour design using the Jovian moons closely follow the invariant manifolds of unstable resonant periodic orbits.<sup>18</sup> Similar investigations in the Sun-Earth<sup>19</sup> and Earth-Moon<sup>20</sup> systems highlight the utility of incorporating natural flow structures arising in multi-body regimes. In this study, the use of periodic orbit solutions in the CR3BP is explored to determine their effect on the converged low-thrust solutions from the optimization process.

In general, the computation of locally fuel-optimal trajectories is posed as an optimal control problem. Possible formulations to solve the problem include both a low-dimension but more sensitive indirect approach using optimal control theory<sup>19,21,22</sup> and a higher-dimension but more robust direct approach.<sup>23–25</sup> A combination of an indirect and a direct method is termed a hybrid optimization algorithm and exploits the relative benefits of both local optimization strategies. For this investigation, the Euler-Lagrange Theorem<sup>26</sup> offers conditions for optimal engine operation, while the commercial optimization packages SNOPT<sup>27</sup> and the simpler function *fmincon* in MATLAB are used to minimize the propellant mass. Two mathematical models of solar electrical propulsion (SEP) are compared: (i) a constant power approximation that simplifies calculations, and (ii) a varying power model as the spacecraft’s distance from the Sun varies. Long-duration transfers are computed using intermediate periodic orbits to seed an initial guess for use in a multiple-shooting scheme; variations in the sequence of intermediate orbits are used to influence the resulting local optimal transfer. Further, the impact of enforcing natural coast arcs associated with periodic orbits is considered within the overall transfer scheme, thus interspersing periods of high thrust where engineering operations are prioritized with coast arcs wherein scientific observations are made. As we will show, coasting arcs generally occur during the most scientifically valuable portions of the trajectories for the specific cases that we consider. By generating low-energy, continuous, end-to-end trajectories for varying transfer geometries to a high-inclination, out-of-ecliptic orbit, the solution space for low-thrust-enabled SmallSats is explored and an analysis on the trajectory characteristics is performed.

## NATURAL MOTION & REFERENCE ORBITS

Physical limitations of the SmallSat platform, particularly mass and volume, place constraints on the available mission architectures for accessing highly out-of-ecliptic orbits. Thus, we restrict our analysis to trajectories that remain at roughly the same distance as Earth from the Sun. In addition to simplifying design considerations for solar arrays and telecommunications systems, this operational paradigm also affords opportunities for close Earth approaches to positively influence the transfer

geometry, reducing propellant mass requirements. However, mathematical models incorporating both the gravitational influence of the Sun and Earth are required to effectively capture the desired multi-body dynamical signature in the optimization scheme.

### Circular Restricted Three-Body Problem

We model the dynamics of the spacecraft using the CR3BP with the Sun and Earth as the primaries. The equations of motion are formulated within the context of a rotating reference frame,  $(\hat{x}, \hat{y}, \hat{z})$ , where  $\hat{x}$  is directed from the Sun to Earth,  $\hat{z}$  is normal to the orbital plane of the primaries and parallel to orbital angular momentum, and  $\hat{y}$  completes the right-handed set. The origin of the coordinate system is the Sun-Earth barycenter. Incorporated into the equations that describe the motion of the spacecraft in this system is the thrust of the Variable Specific Impulse (VSI) engine. The system of equations, including both natural and thrust terms, are nondimensionalized to aid scaling within the numerical integration: computed results are converted to dimensional quantities using characteristic quantities and spacecraft parameter values. The characteristic quantities are defined using the Sun-Earth distance, the mass of the primaries, the characteristic time, and the reference spacecraft mass.<sup>28</sup> The mass parameter  $\mu$  is calculated using

$$\mu = \frac{M_{\oplus}}{M_{\odot} + M_{\oplus}} \quad (1)$$

where  $M_{\odot}$  and  $M_{\oplus}$  are the masses of the Sun and Earth, respectively. The characteristic time is computed as:

$$t^* = \sqrt{\frac{(l^*)^3}{G(M_{\odot} + M_{\oplus})}} \quad (2)$$

where  $l^*$  is the Sun-Earth distance and  $G$  is the universal gravitational constant. The nondimensionalized spacecraft state vector is then defined as:

$$\boldsymbol{\chi} = \begin{Bmatrix} \boldsymbol{r} \\ \boldsymbol{v} \\ m \end{Bmatrix} \quad (3)$$

where  $\boldsymbol{r}$  is the position vector relative to the barycenter,  $\boldsymbol{v}$  is the velocity vector, i.e., the time derivative of  $\boldsymbol{r}$ , as viewed by a rotating observer, and  $m$  is the instantaneous mass of the spacecraft. Note that bold type indicates vector quantities. The equations of motion are then written as:

$$\dot{\boldsymbol{\chi}} = \begin{Bmatrix} \dot{\boldsymbol{r}} \\ \dot{\boldsymbol{v}} \\ \dot{m} \end{Bmatrix} = \begin{Bmatrix} \boldsymbol{v} \\ \boldsymbol{f}_n(\boldsymbol{r}, \boldsymbol{v}) + \frac{T}{m} \boldsymbol{u} \\ -\frac{T^2}{2P} \end{Bmatrix} \quad (4)$$

where  $T$  is thrust magnitude,  $P$  is engine power,  $\boldsymbol{u}$  is a unit vector defining the thrust direction in the rotating frame, and  $\boldsymbol{f}_n$  represents the natural acceleration of the spacecraft. Furthermore, the six-dimensional vector that includes position  $\boldsymbol{r}$  and velocity  $\boldsymbol{v}$  is denoted by the vector  $\boldsymbol{x} = [x \ y \ z \ \dot{x} \ \dot{y} \ \dot{z}]^T$ . The scalar elements of  $\boldsymbol{f}_n$  are then expressed in the rotating frame as:

$$\boldsymbol{f}_n = \begin{Bmatrix} 2\dot{y} + x - \frac{(1-\mu)(x+\mu)}{d_1^3} - \frac{\mu(x+\mu-1)}{d_2^3} \\ -2\dot{x} + y - \frac{(1-\mu)y}{d_1^3} - \frac{\mu y}{d_2^3} \\ -\frac{(1-\mu)z}{d_1^3} - \frac{\mu z}{d_2^3} \end{Bmatrix} \quad (5)$$

where  $d_1$  and  $d_2$  are the distances to the vehicle from the Sun and Earth, respectively:

$$d_1 = \sqrt{(x + \mu)^2 + y^2 + z^2} \quad (6)$$

$$d_2 = \sqrt{(x + \mu - 1)^2 + y^2 + z^2}. \quad (7)$$

The power  $P$  is defined as a scalar value between zero and a maximum available power level specified by the engine model, such that:

$$0 \leq P \leq P_{\max}. \quad (8)$$

In this investigation, the value of  $P_{\max}$  is defined in terms of a reference power level  $P_{\text{ref}}$ , the power available to the SEP system at 1 au. Then, the engine thrust  $T$  is evaluated as:

$$T = \frac{2P}{I_{sp}g_0} \quad (9)$$

where  $I_{sp}$  is the engine specific impulse and  $g_0 = 9.80665 \text{ m/s}^2$ , the gravitational acceleration at the surface of the Earth. In this analysis, system and spacecraft parameters are set equal to the quantities listed in Table 1.

**Table 1. System and SmallSat parameter values.**

Quantity	Value
Solar mass ( $M_{\odot}$ ), kg	$1.9891 \times 10^{30}$
Earth mass ( $M_{\oplus}$ ), kg	$5.9724 \times 10^{24}$
Gravitational Constant (G), $\frac{\text{km}^3}{\text{kg} \cdot \text{s}^2}$	$6.67428 \times 10^{-20}$
Mass parameter ( $\mu$ )	$3.0039 \times 10^{-6}$
Sun-Earth distance ( $l^*$ ), km	$1.4960 \times 10^8$
Characteristic Time ( $t^*$ ), s	$5.0230 \times 10^6$
SmallSat initial wet mass, kg	180
Reference power ( $P_{\text{ref}}$ ) @ 1 au, W	90
Nominal* thrust ( $T$ ), N	0.013
Nominal* specific impulse ( $I_{sp}$ ), sec	1375

\*Nominal values to compare VSI solutions to potential CSI equivalents

## Reference Periodic Orbits

The CR3BP admits a large variety of periodic orbit families, each with unique characteristics that may be suitable for different mission architectures. For example, the vertical families associated with the colinear libration points reliably achieve excursions far above and below the ecliptic plane, i.e., the Sun-Earth invariant plane.<sup>29</sup> Since the goal of this investigation is to achieve high-amplitude motion above the ecliptic plane for the purposes of heliophysics observations and zodiacal dust measurements, the vertical orbit families offer suitable solutions for accomplishing these objectives

due to the large fraction of time that can be spent above the ecliptic by a spacecraft in one of these orbits. To this end, we select the  $L_2$  vertical family for use in our transfer scheme; a sample vertical achieving  $15^\circ$  inclination with respect to the Sun is selected as our destination scientific orbit. In addition, we select  $L_2$  planar Lyapunov orbits as the origin of our transfer sequence because they are readily accessible from a variety of Earth-escape launch conditions.<sup>7-9</sup> Finally, we also use the  $L_2$  axial family to transition between the planar Lyapunovs and the out-of-plane verticals. The axial family, in particular, is useful for bridging the Lyapunov and vertical families because of the bifurcations sequence between the three families.<sup>30</sup>

## TRAJECTORY OPTIMIZATION

A local hybrid optimization scheme is implemented wherein indirect procedures are combined with direct methods to retain low-dimensionality and, therefore, computational efficiency, while increasing the robustness of the convergence process. The application of techniques from calculus of variations supplies conditions on optimal operation of the engine while requiring only the solution for an initial set of co-states. In addition to reducing the number of function evaluations per iteration, this indirect approach also ensures a smooth and continuous control history while not restricting engine operation time histories to an assumed form. A spacecraft mass objective function is locally optimized using a gradient-based procedure, removing a requirement to derive and employ the sensitive transversality conditions of indirect methods.

When a VSI model is employed, the total thrust duration,  $TD$ , must be pre-specified within the two-point boundary value problem (2PBVP). If no limit is placed on either the thrust duration or the mass consumption, the optimization process drives  $TD$  and  $I_{sp}$  to infinity to reduce propellant mass to zero. While restricting  $TD$  is a necessity in the construction of VSI thrust arcs and greatly simplifies the computational aspects of preliminary investigations, we note that low values for thrust  $T$  do correspond to large values for  $I_{sp}$  that are not achievable for current- and near-term low-thrusters. However, when solutions are transformed to equivalent CSI transfers, the time intervals requiring a low level of thrust would correspond to enforced coast arcs.<sup>13</sup> Thus, in this preliminary investigation, we consider only VSI models when constructing low-thrust enabled orbit transfers. Note, however, that we do consider cases of explicitly enforced coast arcs for purposes of scientific observation. Within this investigation, the equivalent  $\Delta V$  cost of a low-thrust transfer arc is computed via:

$$\Delta V = \int_{t_0}^{t_f} \frac{T}{m} dt \quad (10)$$

using numerical quadrature of the thrust and mass profiles. Note that Eq. (10) holds for both CSI and VSI thrust arcs, whether constant or varying power.

### Indirect Optimization of Constant Power Thrust Arcs

When the spacecraft trajectory maintains a relatively constant distance from the Sun, the operating engine power  $P_{\max}$  is assumed to possess a constant value over the duration of the mission, defined as being equipped with an constant-power thruster. For all such constant-power trajectories in this investigation, the maximum engine power is specified as  $P_{\max} = P_{\text{ref}} = 90$  W unless otherwise noted. To fully define the optimization problem, the performance index and the boundary conditions must also be specified. To arrive at the target orbit with the maximum final spacecraft mass for a specified thrust duration, the performance index  $J$  is defined to be the spacecraft mass at

the terminal time of the transfer,  $m_f$ , such that the optimization objective is written

$$\max(J = m_f). \quad (11)$$

The boundary conditions and the Hamiltonian are adjoined to the performance index, such that Eq. (11) is expanded to become the Bolza function

$$\max(J' = m_f + \boldsymbol{\nu}_0^T \boldsymbol{\psi}_0 + \boldsymbol{\nu}_f^T \boldsymbol{\psi}_f + \int_{t_0}^{t_f} [H - \boldsymbol{\lambda}^T \dot{\boldsymbol{\chi}}] dt) \quad (12)$$

where  $H$  is the problem Hamiltonian,  $\boldsymbol{\lambda}$  is a co-state vector, the terms  $\boldsymbol{\psi}$  are vectors comprised of the boundary conditions, and the vector terms involving  $\boldsymbol{\nu}$  are Lagrange multipliers corresponding to the boundary conditions. The subscripts 0 and  $f$  indicate the initial and final times of the transfer. The co-state vector is then

$$\boldsymbol{\lambda} = \begin{Bmatrix} \boldsymbol{\lambda}_r \\ \boldsymbol{\lambda}_v \\ \lambda_m \end{Bmatrix} \quad (13)$$

where  $\boldsymbol{\lambda}_r$  and  $\boldsymbol{\lambda}_v$  are three-dimensional vectors comprised of the position and velocity co-states, respectively, and the scalar  $\lambda_m$  is the mass co-state. The initial and final vector boundary conditions, departure from the starting orbit and arrival at the target orbit, respectively, are

$$\boldsymbol{\psi}_0 = \mathbf{x}_D - \mathbf{x}_D(\tau_0) = \mathbf{0} \quad (14)$$

and

$$\boldsymbol{\psi}_f = \mathbf{x}_T - \mathbf{x}_T(\tau_f) = \mathbf{0} \quad (15)$$

where the subscripts  $D$  and  $T$  indicate the states associated with the departure and target orbits, respectively, and the variables  $\tau$  the corresponding time-like parameters along the orbits. Both boundary conditions in Eqs. (14) and (15) are satisfied by solving the boundary value problem for matching position and velocity states between the natural periodic orbits ( $\mathbf{x}_D(\tau_0)$  and  $\mathbf{x}_T(\tau_f)$ ) and the beginning or end of the corresponding thrust segments ( $\mathbf{x}_D$  and  $\mathbf{x}_T$ ).

Calculus of variations is employed to define several properties of the 2PBVP and to acquire the derivatives of the co-states. The Hamiltonian of the problem is set equal to

$$H = \boldsymbol{\lambda}^T \dot{\boldsymbol{\chi}} = \boldsymbol{\lambda}_r^T \mathbf{v} + \boldsymbol{\lambda}_v^T \left[ \mathbf{f}_n(t, \mathbf{r}, \mathbf{v}) + \frac{T}{m} \mathbf{u} \right] - \lambda_m \frac{T^2}{2P} \quad (16)$$

where the value of  $H$  is constant over the trajectory for the time invariant CR3BP. The optimal control strategy emerges by maximizing the Hamiltonian with respect to the controls  $T$ ,  $P$ , and  $\mathbf{u}$  such that

$$P = P_{\max} \quad (17)$$

$$T = \frac{\lambda_v P_{\max}}{\lambda_m m} \quad (18)$$

$$\mathbf{u} = \frac{\boldsymbol{\lambda}_v}{\lambda_v} \quad (19)$$

where  $\lambda_v = \|\boldsymbol{\lambda}_v\|$ . The Euler-Lagrange conditions for optimality modify the performance index in Eq. (12). With the Hamiltonian, Eq. (16), and the controls in Eqs. (17)-(19), the following

differential equations govern the co-states:

$$\dot{\lambda} = -\left(\frac{\partial H}{\partial \chi}\right)^T = \begin{Bmatrix} -\lambda_v^T \left(\frac{\partial f_n}{\partial r}\right) \\ -\lambda_r^T - \lambda_v^T \left(\frac{\partial f_n}{\partial v}\right) \\ \lambda_v \frac{T}{m^2} \end{Bmatrix} \quad (20)$$

where the initial state for  $\lambda_m$  is set equal to unity to reduce the number of variables. Note that: (a) a similar procedure to minimize the initial mass for a given target mass results in identical conditions for engine operation, and (b) the differential equations for the co-states do not change form based upon the underlying natural dynamics; thus,  $\frac{\partial f_n}{\partial r}$  and  $\frac{\partial f_n}{\partial v}$  are freely substituted when using models of varying fidelity.<sup>31,32</sup>

### Indirect Optimization of Varying Power Thrust Arcs

The development of the operational conditions for a varying engine power system, e.g., SEP, proceeds similarly to the indirect method for constant-power thrusters. In contrast, however, the maximum available engine power is now determined via

$$P_{\max} = \frac{P_{\text{ref}}}{d_{\odot}^2} \quad (21)$$

where  $d_{\odot}$  is the nondimensional distance between the spacecraft and the Sun;  $d_{\odot} = d_1$  in the Sun-Earth CR3BP. Under this power law, the spacecraft possesses a nominal operating power of 90 W at one Earth distance from the Sun, but the available engine power is not constrained by any upper or lower limits.

The objective function and constraints for a varying power system are the same as for constant-power engines; thus, Eqs. (11)-(15) are unchanged in the definition of the 2PBVP. Recalling from Eq. (17) that the most efficient engine operation occurs at the maximum available power level, the new problem Hamiltonian is then written as:

$$H = \lambda^T \dot{\chi} = \lambda_r^T v + \lambda_v^T \left[ f_n(t, r, v) + \frac{T}{m} u \right] - \lambda_m \frac{T^2 d_{\odot}^2}{2P_{\text{ref}}} \quad (22)$$

As before, maximizing the Hamiltonian produces the primer vector in Eq. (19) and the thrust magnitude control is evaluated as

$$T = \frac{\lambda_v P_{\text{ref}}}{\lambda_m m d_{\odot}^2} \quad (23)$$

while the Euler-Lagrange conditions yield the following co-state equations of motion

$$\dot{\lambda} = -\left(\frac{\partial H}{\partial \chi}\right)^T = \begin{Bmatrix} -\lambda_v^T \left(\frac{\partial f_n}{\partial r}\right) + \lambda_m \frac{T^2}{P_{\text{ref}}} d_{\odot} \\ -\lambda_r^T - \lambda_v^T \left(\frac{\partial f_n}{\partial v}\right) \\ \lambda_v \frac{T}{m^2} \end{Bmatrix} \quad (24)$$

where  $d_{\odot}$  is the position vector from the Sun to the spacecraft ( $d_{\odot} = d_1$  in the Sun-Earth CR3BP). Consistent with a constant-power thrust arc, the engine operating conditions and the differential equations are unchanged if the initial mass is minimized or if differing models of the natural dynamics are incorporated.

## Constructing Initial Guesses for Orbit Sequences

Prior to generating a complete transfer from an initial, low-inclination orbit to a high-inclination, science orbit, an initial guess for the trajectory is constructed using periodic orbits within the Sun-Earth system to seed the low-thrust segments. These periodic orbits are selected by analyzing the evolution of and bifurcations that occur along natural periodic orbit families within the Sun-Earth system.\*

Specifically, the Sun-Earth  $L_2$  Lyapunov, axial, and vertical orbit families tend to increase in maximum inclination with respect to the Sun as the energy of the orbit families increases, permitting use of this trend when designing efficient transfers to high-inclination vertical orbits. The  $L_2$  Lyapunov orbit selected as the initial orbit possesses a Jacobi constant of 3.0005. Conversely, the final science orbit is selected from the Sun-Earth  $L_2$  vertical orbit family. Along these orbits, a spacecraft spends a significant fraction of the orbital period located at high inclinations with respect to the ecliptic, affording observations of the Sun's polar regions and of the zodiacal dust cloud.<sup>29</sup> To satisfy the  $15^\circ$  condition for which scientific observations can be performed, an  $L_2$  vertical orbit with a Jacobi constant of 2.93 and a maximum inclination of  $15.24^\circ$  with respect to the Sun is used as the final science orbit. These two orbits form the Jacobi constant boundaries from which intermediate orbits are selected to form the initial guess. By constructing the initial guess to transition from a low-energy orbit to a high-energy orbit using orbits with energies within the bounds of the initial and final orbits, a low-thrust-enabled spacecraft can gradually raise its energy while also leveraging the natural dynamics that exist within the Sun-Earth system.

Since the initial and final orbits possess a large difference in their Jacobi constants, numerous intermediate orbits are used in the initial guess to allow the low-thrust engine the necessary time to both raise the energy of the spacecraft and change the geometry of the trajectory to insert into the desired vertical orbit from a planar periodic orbit. For this study, the orbits drawn from the  $L_2$  axial family act as transitional segments through which the low-thrust engine can induce out-of-plane motion prior to reaching the vicinity of the  $L_2$  vertical family. By drawing orbits from each family to serve as intermediate orbits when constructing the initial guess, a path is formed which utilizes the fundamental dynamical structures that exist within the CR3BP to guide the optimization algorithm to a mass-efficient transfer.

Altering the number of initial guess orbits that are selected from the Sun-Earth  $L_2$  Lyapunov,  $L_2$  axial, and  $L_2$  vertical families inherently affects the local solution upon which the optimization algorithm converges. The intermediate orbits are selected at equal intervals in the Jacobi constant along each family. For example, a sequence denoted **L:2-A:2-V:11** indicates that the initial guess includes:

- **L:2** - the originating  $L_2$  Lyapunov orbit as well as a second  $L_2$  Lyapunov orbit interspaced between the starting orbit and the orbit at which the bifurcation with the  $L_2$  axial family occurs;
- **A:2** - two distinct  $L_2$  axial orbits with Jacobi constants linearly spaced between the  $L_2$  axial family's bifurcations with the  $L_2$  Lyapunov and  $L_2$  vertical families; and,
- **V:11** - ten intermediate  $L_2$  vertical orbits with Jacobi constants ranging between the Jacobi constant of the  $L_2$  vertical family's bifurcation with the  $L_2$  axial family and 2.93, along with

---

\*See Grebow<sup>30</sup> for a related discussion within the Earth-Moon CR3BP model.

the final orbit with a Jacobi constant of 2.93.

An illustration of this initial guess is portrayed in Figure 1(a) where the red arc denotes the initial periodic orbit, the intermediate orbits are plotted in gold, and the final periodic orbit is represented in blue. An additional perspective focused on the lower-inclination Lyapunov and axial orbits is presented in Figure 1(b) with the same configuration. All transfers presented in this paper follow this naming convention with varying numbers of intermediate orbits forming the initial guess for the final transfer.

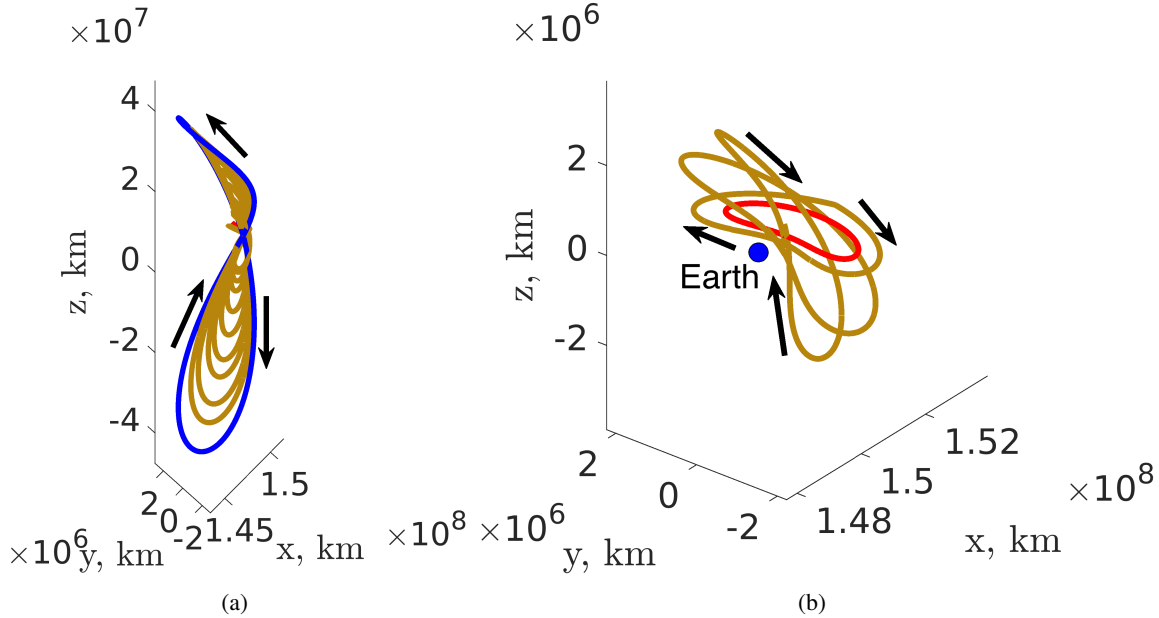


**Figure 1. Initial guess for a L:2-A:2-V:11 Lyapunov to vertical orbit transfer in the Sun-Earth rotating frame in dimensional coordinates: (a) spatial view and (b) Lyapunov and axial segments only. Low-thrust segments are displayed in gold, the final periodic orbit in blue, and red depicts the initial periodic orbit**

## TRANSFER SEQUENCES ACCESSING HIGH-INCLINATION ORBITS

Using the approach outlined in the previous section to construct the initial guess for a transfer to a high-inclination vertical orbit, continuous solutions feasible for an ESPA-class SmallSat with the parameters given in Table 1 are developed. Initially, a transfer is designed assuming a constant power level VSI engine for the Sun-Earth  $L_2$  Lyapunov to  $L_2$  vertical transfer prior to developing an equivalent varying power level VSI transfer. In addition to generating transfers with continuous VSI operation, transfers with coast arcs replacing the thrust arcs at the maxima of the intermediate vertical-like arcs along the transfer are designed. These enforced-coast transfers leverage the periods of minimal thrust that are efficiently revealed by the application of the Euler-Lagrange equations. These coast arcs permit periods of scientific observations throughout the transfer while also not considerably affecting the geometry and propellant requirements of the mission. For a SmallSat, coast arcs permit periods of performing scientific observations that may be sensitive to low-thrust engine operation as well as improving the amount of power that can be delegated to the science

instruments. Finally, a comparison of the characteristics of many transfers of differing geometries is presented.

### Fully VSI Transfer Sequences

A continuous solution is developed for the **L:2-A:2-V:11** Sun-Earth  $L_2$  Lyapunov to  $L_2$  vertical transfer assuming a constant power level of 90 W using SNOPT and the initial guess displayed in Fig 1. The final, end-to-end trajectory is depicted in Figure 2 in both isometric and top-down views in the Sun-Earth rotating frame using dimensional coordinates and a color scheme consistent with Figure 1. First, the trajectory follows the initial Lyapunov orbit, depicted in red, prior to beginning the low-thrust burn and following a path that resembles the Lyapunov orbits with an increasing out-of-plane component. Once the Jacobi constant of the trajectory has been lowered to the value necessary to transition to motion similar to the vertical orbit family, the trajectory employs varying levels of thrust while following the  $L_2$  vertical family profile before ultimately reaching the necessary energy to insert into the final science orbit. Both figures reveal that the converged trajectory approximately follows the intermediate orbits used to construct the initial guess thereby demonstrating the value in using dynamical systems theory for initial guess design. For an ESPA-class SmallSat with the parameters given in Table 1, this trajectory requires a total transfer duration of 11.80 years and 43.26 kg of propellant.

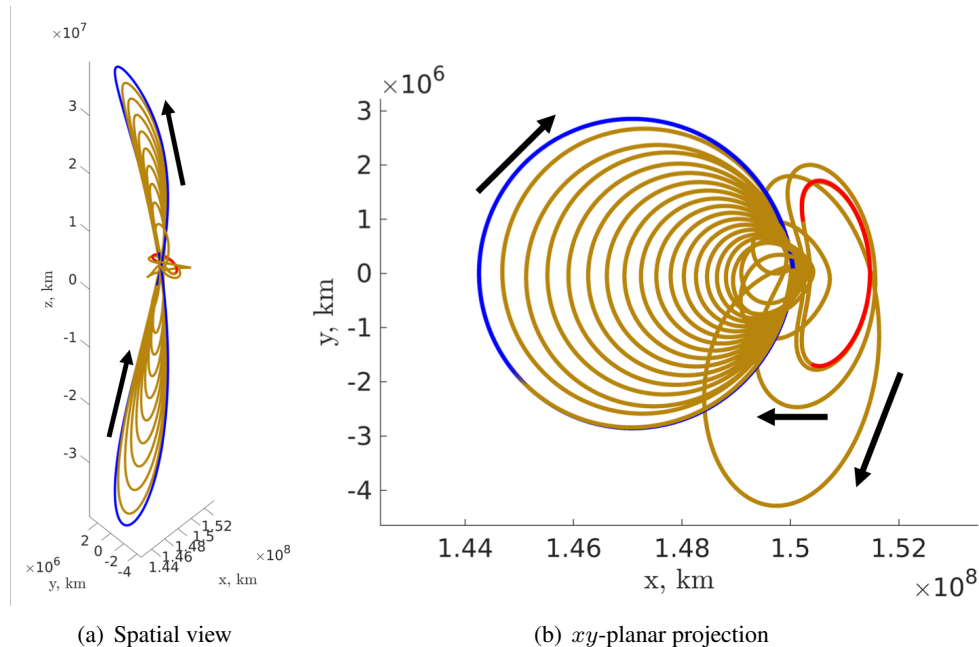


**Figure 2. Low-thrust trajectory delivering a SmallSat to a high-inclination vertical orbit. Low-thrust segments are displayed in gold, the final periodic orbit in blue, and red depicts the initial periodic orbit**

In addition to analyzing the TOF and required propellant mass, the thrust profile can also be examined to determine the feasibility of this transfer for a SmallSat. The thrust profile for the entire transfer is displayed in Figure 3(a) in gold while the black dashed line indicates the thrust limit given current technological capabilities for this class of SmallSat. This thrust profile falls well below the nominal thrust threshold for an equivalent CSI engine, demonstrating that the required

thrust magnitude is achievable with current SmallSat technology. Then, Figure 3(b) depicts the out-of-plane angle of the trajectory with respect to the ecliptic. The change in the maximum out-of-plane angle is approximately linear in time with each year adding an additional  $1^\circ$  of maximum inclination to the transfer. Furthermore, the minima of the thrust magnitudes generally match the maxima of the out-of-plane angle, suggesting that minimal thrusting is occurring at the high out-of-plane components of the transfer. This observation implies that these high out-of-plane segments could be replaced by coast arcs with limited impact on the trajectory.

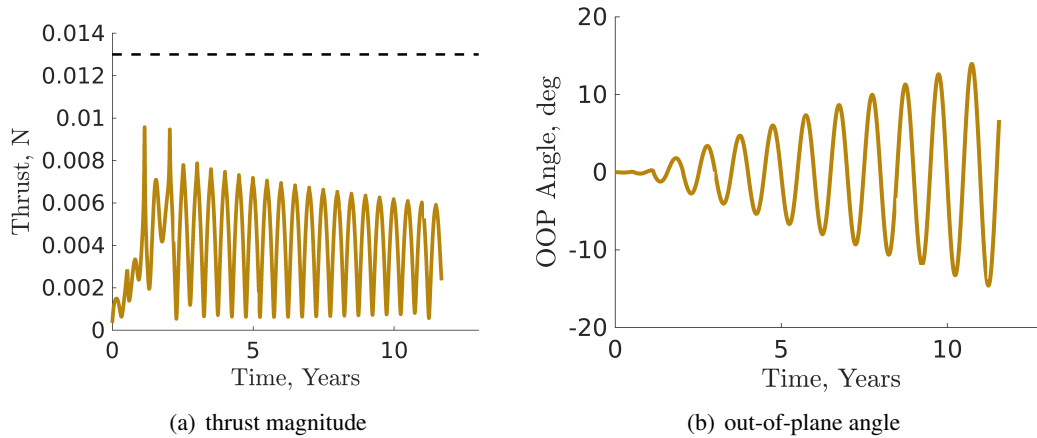


**Figure 3. Low-thrust trajectory characteristics for delivering a SmallSat to a high-inclination vertical orbit**

### Transfer Sequences with Varying Power Levels

A transfer designed with a constant power assumption is used as an initial guess for a transfer that incorporates a propulsion system with varying electrical power due to changes in the distance of a spacecraft from the Sun. In general, the power available to the spacecraft is expected to decrease below the  $P_{\max} = 90$  W assumption at 1 au across most of the trajectory due to the use of  $L_2$  periodic orbit families, with distances exceeding 1 au and up to 1.005 au from the Sun. However, by using the optimized, constant power transfer as an initial guess, less computational effort is required to converge on a new, varying power transfer. Employing the constant power initial guess, the converged solution for a varying power **L:2-A:2-V:11** transfer appears in Figure 4(a) with a configuration and color scheme consistent with Figure 1. For this transfer, the TOF and propellant mass required are 11.80 years and 43.07 kg, respectively. Additionally, a planar perspective is depicted in Figure 4(b) exhibiting similar motion to the constant power **L:2-A:2-V:11** transfer. This similarity in transfer geometry confirms the value of using the constant power assumption to develop end-to-end solutions that are approximately retained in a higher fidelity power model.

The effect of varying power available to the spacecraft is revealed in Figure 5(a) which depicts oscillations in power throughout the transfer sequence. Examining these power fluctuations and the trajectory above, closer passes below 1 au with respect to the Sun, are performed, which consequently raise the available power to the engine above the nominal 90 W threshold at 1 au, increasing the performance of the engine when feasible. Additionally, the thrust magnitude history of the transfer is displayed in Figure 5(b) with the black dashed line representing the nominal thrust for a CSI equivalent engine. Thus, the required thrust for this solution is within current SmallSat technologi-

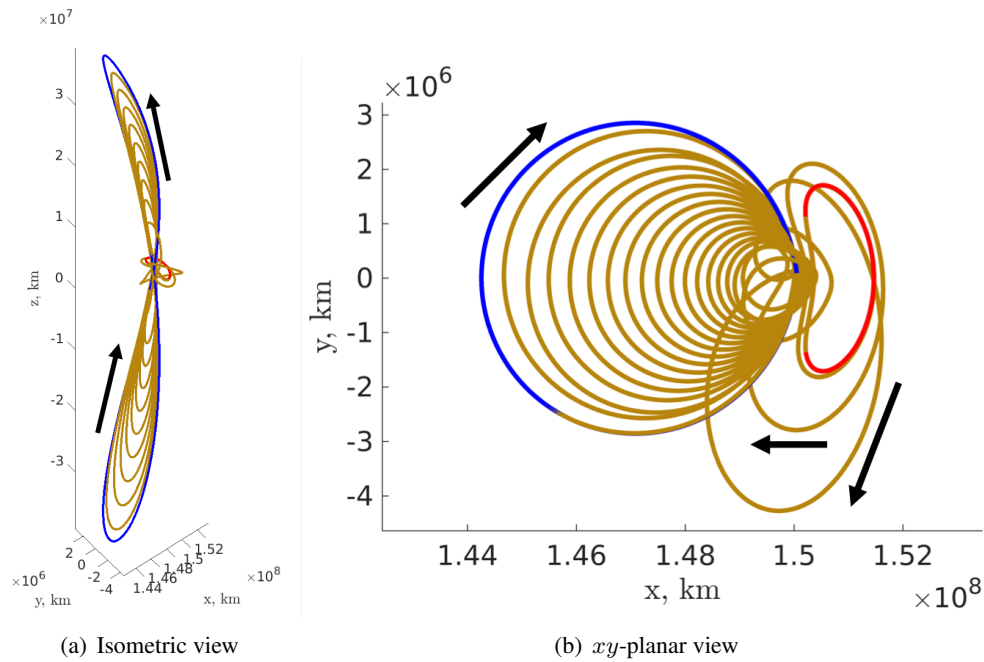


**Figure 4. Low-thrust varying power level trajectory delivering a SmallSat to a high-inclination vertical orbit. Low-thrust segments are displayed in gold, the final periodic orbit in blue, and red depicts the initial periodic orbit**

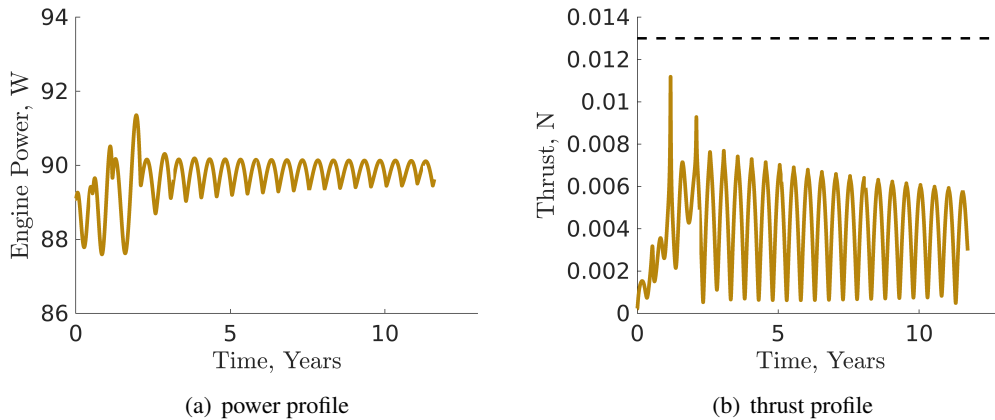


**Figure 5. Low-thrust varying power trajectory characteristics for delivering a Small-Sat to a high-inclination vertical orbit**

cal capabilities. However, there are certain operational constraints that may encourage coast arcs or other geometries to be explored.

### Sequences Integrating Coast Arcs

While assuming a single, long thrust arc to transfer from the initial orbit to the final orbit does offer some benefits for the trajectory design process, it is not operationally feasible and can prevent valuable scientific observations from being performed. Furthermore, if coast arcs are enforced at the

higher amplitude segments of the transfer then scientific objectives may still be realized while also not significantly impacting the TOF and propellant mass requirements. To incorporate coast arcs into the trajectory, the converged, constant power level **L:2-A:2-V:11** solution is used as an initial guess where the high amplitude thrust segments that were originally formed from the intermediate vertical orbits are transitioned to natural coast arcs. Furthermore, the coast arcs are allowed to vary in duration to ensure convergence on an optimal end-to-end solution. The continuous, constant power level solution is displayed in Figure 6(a) in the Sun-Earth rotating frame in dimensional coordinates where the initial periodic orbit arc is in red, gold depicts the low-thrust arcs, blue represents the final periodic orbit, and the coast segments are colored light blue. A planar projection of the transfer appears in Figure 6(b), where the solution incorporating coast arcs exhibits a similar geometry to the continuous thrust VSI, constant power level transfer in Figure 2(a). This transfer requires 44.69 kg of propellant and a TOF of 11.81 years demonstrating that the trajectory characteristics are only negligibly affected by enforcing coast arcs within the transfer. Note that each coast arc is roughly 1.5 months in duration.

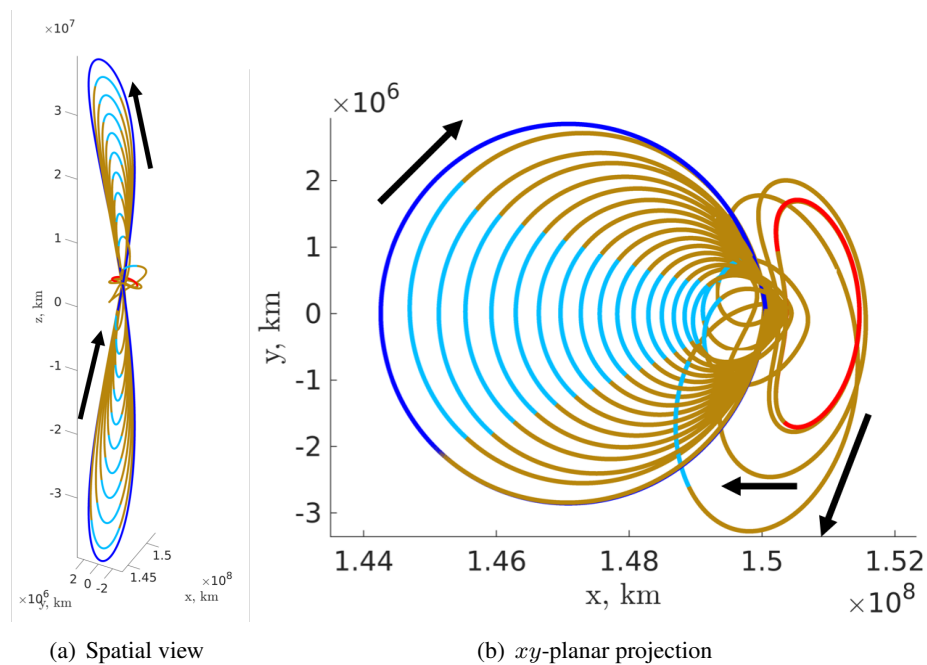


**Figure 6. Low-thrust, constant power level trajectory with coast arcs delivering a SmallSat to a high-inclination vertical orbit. Low-thrust segments are displayed in gold, the final periodic orbit in blue, red depicts the initial periodic orbit, and the coast arcs are in orange**

The thrust magnitude history depicted in Figure 7(a) exhibits similar properties to the thrust magnitude history depicted in Figure 3(a). The maximum thrust value is slightly larger for this VSI transfer with coast arcs, but remains well under the 13 mN nominal thrust CSI equivalent engine, suggesting that the transfer incorporating thrust arcs may be a feasible transfer given current Small-Sat technological capabilities. Additionally, the out-of-plane angle along this transfer is illustrated in Figure 7(b) where gold denotes thrust segments and light blue represents coast arcs. The out-of-plane angle exhibits similar behavior to the fully VSI, constant power level transfer, but in the transfer with integrated coast arcs, the coast arcs correspond to segments with the highest out-of-

ecliptic motion reinforcing that science can be performed throughout this transfer. In both instances, the maximum out-of-plane angles reached along each high amplitude pass increase linearly with time by approximately  $1^\circ$  every year. Although the required propellant mass is slightly larger than the transfer using only thrust segments with a constant power level, some coast arcs could be removed from the above transfer, particularly coast arcs at smaller inclinations, to potentially reduce the required propellant mass while still performing science observations during the coast arcs at the higher out-of-plane amplitudes. However, while the flight time, propellant mass, and out-of-plane angle relationships have been demonstrated to hold for the **L:2-A:2-V:11** transfer, additional transfer geometries must be developed to more fully explore the trajectory design space for accessing a high-inclination,  $15^\circ$  vertical orbit.

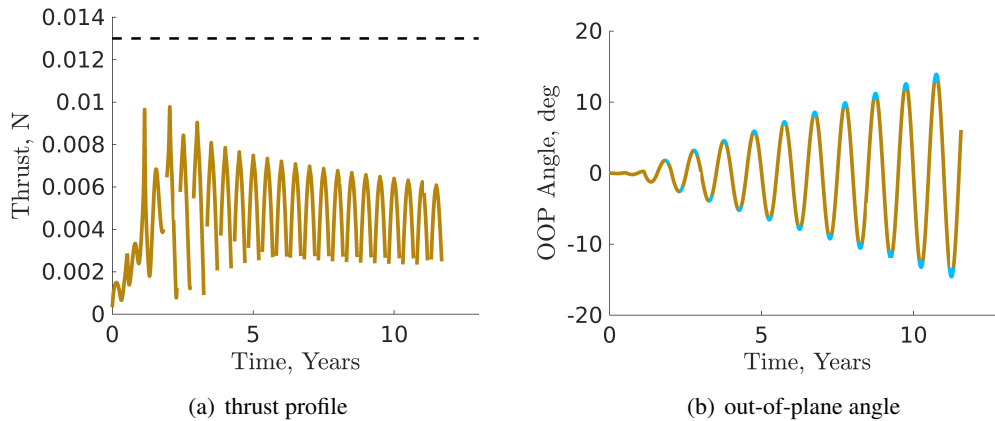


**Figure 7. Low-thrust trajectory with enforced coast arcs characteristics for delivering a SmallSat to a high-inclination vertical orbit**

### Exploration of Transfers with Distinct Geometries

Using the presented method to construct initial guesses for additional transfers by modifying the intermediate orbit sequence, end-to-end solutions are developed for a variety of geometries. These geometries include at most three Lyapunov orbits, five axial orbits, and twelve vertical orbits with many transfers including less than these values. In all, 43 converged transfers are developed with differing flight times, propellant mass requirements, and thrust profiles. Further, several of the continuous, fully VSI solutions are then transitioned to incorporate coast arcs so that an additional 11 converged solutions with coast arcs at high amplitudes are included.

The flight time and propellant mass trade space is explored to determine whether additional insights into the solution space may be uncovered. Figure 8 displays the relationship between TOF and propellant mass requirements for all of the generated transfers, with constant power VSI transfers colored red, constant power VSI transfers with coast arcs in blue, and the black dashed line represents the initial mass of the spacecraft, 180 kg. Furthermore, grey dashed lines connect fully VSI transfers and VSI transfers with integrated coast arcs that possess the same transfer geometry, e.g., **L:2-A:2-V:11**. Analysis of this figure reveals that the TOF and required propellant mass are inversely related: longer flight times generally correspond with lower propellant mass usage and higher deliverable mass fractions. Interestingly, this relationship is not exact; some transfers possess lower flight times and propellant mass usage than other nearby transfers, an artifact of the

transfer geometry of each initial guess and the local basins of convergence that they fall within. Nevertheless, there is a Pareto front characterizing the trade-off between propellant usage and transfer duration. This front is significantly below the initial spacecraft mass and can be attributed to the large difference in energy between the initial orbit and final orbit. This energy difference and the relationship between TOF and propellant mass usage demonstrates that while there is a minimum propellant mass required for a low-thrust-enabled SmallSat to complete this transfer, the trade space may be explored for a particular mission scenario to reduce the amount of propellant required.

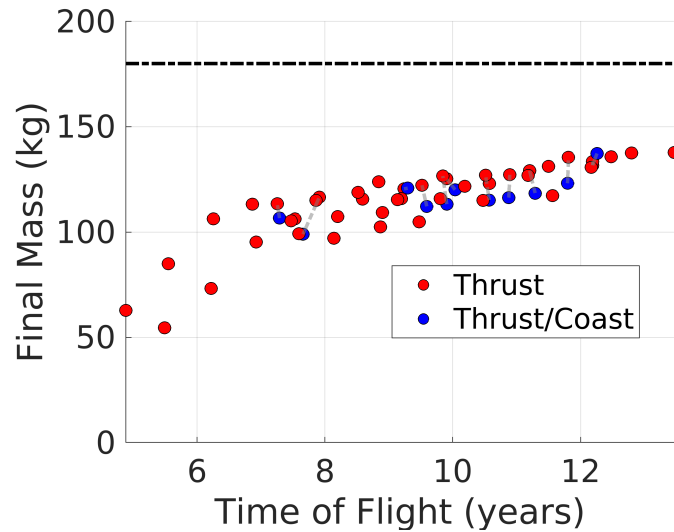


**Figure 8. Required propellant mass vs. flight time for delivering a SmallSat to a 15° vertical orbit using distinct transfer geometries**

The  $\Delta V$  and TOF relationship offers valuable insights into the solution space for transfers to high-inclination vertical orbits. Figure 9 depicts the  $\Delta V$  and TOF relationship with a configuration and color scheme consistent with Figure 8. Analysis of this figure reveals that the transfers with integrated coast arcs all possess lower equivalent  $\Delta V$  requirements than the fully VSI transfers that they were developed from. Furthermore, the VSI transfers with longer flight times generally also exhibit less variance in their equivalent  $\Delta V$  requirement. However, even for transfers with distinct geometries but nearly identical flight times, large differences in the equivalent  $\Delta V$  occur, suggesting that these transfers correspond to distinct local minima. This observation justifies a thorough exploration of the solution space where multiple transfer geometries are analyzed in order to determine the ideal transfer given mission and operational constraints.

The flight time and propellant mass usage for each transfer are examined as a function of the number of intermediate orbits for further insights into the solution space. The number of intermediate orbits is defined as the number of orbits leveraged in constructing the initial guess, excluding the initial and final orbits. Figure 10(a) illustrates the relationship between the TOF and number of intermediate orbits with a configuration and color scheme consistent with Figure 8. Additionally, Figure 10(b) depicts the final mass and number of intermediate orbits relationship for all of the generated transfers. Examining these figures reveals that the final converged solution has a significant dependence on the initial guess input to the optimization algorithm. As expected, increasing the number of orbits generally increases the overall time of flight with variations depending on the particular combination of orbit sequences that were chosen. This result indicates that the optimizer

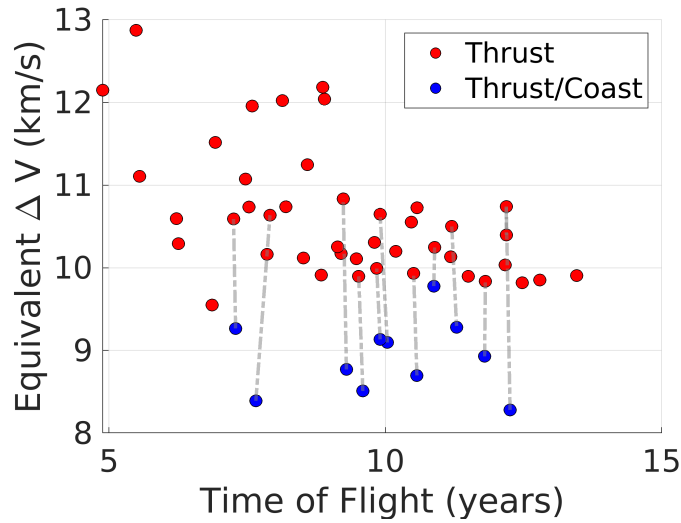


**Figure 9. Equivalent  $\Delta V$  vs. flight time for delivering a SmallSat to a  $15^\circ$  vertical orbit using distinct transfer geometries**

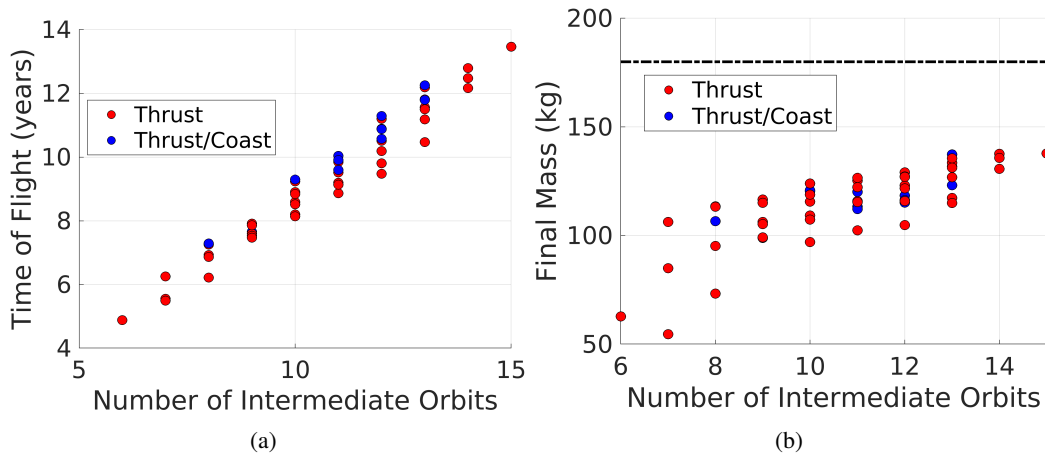


**Figure 10. Relationship between the number of intermediate orbits used to construct the initial guess for: (a) flight time and (b) propellant mass usage**

tends to fall into a local basin of convergence that relies heavily on the topology of the initial guess. A similar effect is seen with the final optimized mass, although as the number of orbits is increased to a large integer value, the gains in the final mass become less significant. These results imply that examining a variety of low-energy trajectory geometries for these types of transfers can result in significant improvements in the final optimized mass along with new trajectory solutions.

## CONCLUSION

In this investigation, we have designed transfer solutions to highly out-of-ecliptic orbits within the constraints of expected SmallSat propulsion capabilities, enabling scientific investigations of the zodiacal dust cloud as well as the polar regions of the Sun. In particular, a scientific orbit with an inclination of  $15^\circ$  may be reached by exploiting the multi-body dynamics of the Sun and the

Earth as well as solar electric low-thrust propulsion. Initial guesses are seeded with low-energy orbits, particularly  $L_2$  Lyapunovs, axials, and verticals, resulting in converged transfer solutions with flight times ranging from 4 to 14 years and requiring propellant masses 125 kg to 40 kg, respectively, out of an initial spacecraft mass of 180 kg. Though a variable specific impulse engine model was used in this investigation, the results are compared to expected performance of equivalent constant specific impulse systems; explicit contrasts between the two engine models warrant future investigation. Also, this investigation primarily assumes a constant power available to the SEP engine, though equivalent optimized trajectories using varying power models are also developed and exhibit comparable operational characteristics.

A variety of transfer scenarios and geometries were considered, primarily via the selection of different sequences of baseline low-energy orbits seeding the initial guess of the hybrid optimization scheme. The results are consistent with a multi-modal trade space with many basins of local optima: optimized end-to-end solutions are heavily influenced by the initial guess. Further comparison is performed between transfers allowing engine operation throughout and transfers with enforced coast arcs at highly out-of-plane portions of the trajectory. Since these enforced coasts correspond to valleys in the VSI thrust profile, fully thrusting and enforced coasting transfers exhibit similar propellant consumption, time of flight, and transfer geometry. However, these enforced coasts correspond to the most scientifically valuable periods along the trajectory, presenting a mutually beneficial trade-off between science and engineering considerations: the spacecraft performs scientific observations when well out of the ecliptic plane then alternates thrust arcs when closer to the gravitational influence of the Earth.

Several avenues for future work are available, including a more systematic exploration of the available trade space between planar trajectories and highly out-of-plane science orbits. While a variety of transfer geometries are considered in this investigation, incorporation of additional periodic orbit families and differing sequences would further illuminate the available transfer options. More detailed definition of the initial mission phases is also warranted; depending of the launch conditions, periods of time in the Earth-Moon system may be required prior to entering heliocentric regimes. As previously noted, transitioning between varying and constant specific impulse solutions is needed for near-term realization of feasible trajectories. Further exploration of the enforced coasting paradigm is warranted, especially as it presents a natural trade between science objectives and engineering requirements.

## ACKNOWLEDGMENT

This research was carried out at the Jet Propulsion Laboratory, California Institute of Technology, under a contract with the National Aeronautics and Space Administration.

## REFERENCES

- [1] B. H. May, "A Survey of Radial Velocities in the Zodiacal Dust Cloud," Ph.D. Dissertation, Department of Physics, Imperial College, London, 2007. <https://spiral.imperial.ac.uk/bitstream/10044/1/1333/1/May-BH-2007-PhD-Thesis.pdf>.
- [2] W. T. Reach, B. A. Franz, and J. L. Weiland, "The Three-Dimensional Structure of the Zodiacal Dust Bands," *Icarus*, Vol. 127, 1997, pp. 461–484. Article No. IS975704.
- [3] K. Wenzel, "The Ulysses Mission - A Voyage to the Poles of the Sun," *Nuclear Physics B - Proceedings Supplements*, Vol. 39, February 1995, pp. 59–68. [https://doi.org/10.1016/0920-5632\(95\)00007-V](https://doi.org/10.1016/0920-5632(95)00007-V).
- [4] NASA. NASA Ulysses Mission Website, 2018. <https://solarsystem.nasa.gov/missions/ulysses/in-depth/>; Accessed 15 July 2019.

- [5] ESA. ESA Ulysses Mission Website, 2019. <https://www.cosmos.esa.int/web/ulysses/the-ulysses-mission>; Accessed 15 July 2019.
- [6] California Polytechnic State University, *CubeSat Design Specification*, 13 ed., February 20 2014. Accessed at: <http://www.cubesat.org/resources/>.
- [7] F. Alibay, N. Bosanac, and J. R. Stuart, "A Low-Thrust-Enabled SmallSat Heliophysics Mission to Sun-Earth  $L_5$ ," *IEEE Aerospace Conference*, Big Sky, Montana, March 3-10 2018.
- [8] I. Elliott, C. Sullivan, N. Bosanac, J. R. Stuart, and F. Alibay, "Designing Low-Thrust Enabled Trajectories for a Heliophysics SmallSat Mission to Sun-Earth  $L_5$ ," *AAS/AIAA Space Flight Mechanics Meeting*, Ka'anapali, Maui, Hawaii, January 13-17 2019. AAS 19-266.
- [9] C. Sullivan, I. Elliott, N. Bosanac, F. Alibay, and J. R. Stuart, "Exploring the Low-Thrust Trajectory Design Space for SmallSat Missions to the Sun-Earth Triangular Equilibrium Points," *AAS/AIAA Space Flight Mechanics Meeting*, Ka'anapali, Maui, Hawaii, January 13-17 2019. AAS 19-267.
- [10] D. Goebel, J. Brophy, J. Polk, I. Katz, and J. Anderson, "Variable Specific Impulse High Power Ion Thruster," *Joint Propulsion Conference*, Tucson, Arizona, AIAA/ASME/SAE/ASEE, July 2005. Paper No. AIAA 2005-4246.
- [11] T. W. Glover, F. R. C. Diaz, A. V. Ilin, and R. Vondra, "Projected Lunar Cargo Capabilities of High-Power VASIMR Propulsion," *Proceedings of 30th International Electric Propulsion Conference*, Florence, Italy, September 2007. IEPC-2007-244.
- [12] K. Komurasaki, Y. Arakawa, and H. Takegahara, "An Overview of Electric and Advanced Propulsion Activities in Japan," *Proceedings of Third International Conference of Spacecraft Propulsion*, Cannes, France, October 2000, pp. 27–39.
- [13] A. Das-Stuart, K. C. Howell, and D. Folta, "Rapid Trajectory Design in Complex Environments Enabled by Reinforcement Learning and Graph Search Strategies," 2019. Available Online April 25, 2019, <https://dx.doi.org/10.1016/j.actaastro.2019.04.037>.
- [14] G. J. Whiffen, "Static/Dynamic Control for Optimizing a Useful Objective," U. S. Patent 6,496,741, December 17 2002.
- [15] G. J. Whiffen, "An Investigation of a Jupiter Galilean Moon Orbiter Trajectory," *AAS/AIAA Astrodynamics Specialist Conference*, Big Sky, Montana, August 3-7 2003. AAS Paper 03-544.
- [16] G. J. Whiffen, "Mystic: Implementation of the Static Dynamic Optimal Control Algorithm for High Fidelity Low Thrust Trajectory Design," *AIAA/AAS Astrodynamics Specialists Conference*, Keystone, Colorado, August 21-24 2006. AIAA-2006-6741.
- [17] M. W. Lo, "The Interplanetary Superhighway and the Origins Program," *Aerospace Conference Proceedings (2002)*, *IEEE*, Vol. 7, Big Sky, Montana, March 9-16 2002, pp. 3543–3562.
- [18] R. L. Anderson and M. W. Lo, "Role of Invariant Manifolds in Low-Thrust Trajectory Design," *Journal of Guidance, Control, and Dynamics*, Vol. 32, November-December 2009, pp. 1921–1930.
- [19] J. Senent, C. Ocampo, and A. Capella, "Low-Thrust Variable-Specific-Impulse Transfers and Guidance to Unstable Periodic Orbits," *Journal of Guidance, Control, and Dynamics*, Vol. 28, March-April 2005, pp. 280–290.
- [20] J. R. Stuart, M. T. Ozimek, and K. C. Howell, "Optimal, Low-Thrust, Path-Constrained Transfers between Libration Point Orbits using Invariant Manifolds," *AIAA/AAS Astrodynamics Specialist Conference*, Toronto, Ontario, August 2-5 2010.
- [21] M. Volle, "Optimal Variable-Specific-Impulse Rendezvous Trajectories Between Halo Orbits," *International Symposium on Space Flight Dynamics*, Kanazawa, Japan, Japan Society for Aeronautical and Space Sciences and ISTS, June 2006. Paper No. ISTS 2006-d-73.
- [22] R. Russell, "Primer Vector Theory Applied to Global Low-Thrust Trade Studies," *Journal of Guidance, Control, and Dynamics*, Vol. 30, March-April 2007, pp. 460–473.
- [23] G. Mingotti, F. Topputo, and F. Bernelli-Zazzera, "Combined Optimal Low-Thrust and Stable-Manifold Trajectories to the Earth-Moon Halo Orbits," *New Trends in Astrodynamics and Applications III*, Vol. 886, February 2007, pp. 100–112.
- [24] C. Martin and B. Conway, "Optimal Low-Thrust/Invariant Manifold Earth Moon Transfer Trajectories," *Space Flight Mechanics Meeting*, San Diego, California, AAS/AIAA, February 2010, pp. 89–106. Paper No. AAS 10-105.
- [25] J. Betts, "Survey of Numerical Methods for Trajectory Optimization," *Journal of Guidance, Control, and Dynamics*, Vol. 21, March-April 1998, pp. 193–207.
- [26] A. E. Bryson, Jr. and Y.-C. Ho, *Applied Optimal Control*. Waltham, Massachusetts: Blaisdell Publishing, 1969.
- [27] P. E. Gill, W. Murray, and M. A. Saunders, "SNOPT: An SQP algorithm for large-scale constrained optimization," *Society for Industrial and Applied Mathematics Journal of Optimization*, Vol. 12, No. 4, 2002, pp. 979–1006.

- [28] V. Szebehely, *Theory of Orbits*. New Haven, Connecticut: Academic Press, first ed., 1967.
- [29] D. Dichmann, E. Doedel, and R. Paffenroth, "The Computation of Periodic Solutions of the 3-Body Problem Using the Numerical Continuation Software AUTO," *International Conference on Libration Point Orbits and Applications*, Aiguablava, Spain, June 10-14 2002.
- [30] D. J. Grebow, "Generating Periodic Orbits in the Circular Restricted Three-Body Problem with Applications to Lunar South Pole Coverage," M.S. Thesis, School of Aeronautics and Astronautics, Purdue University, West Lafayette, Indiana, 2006.
- [31] J. R. Stuart, K. C. Howell, and R. S. Wilson, "Design of End-To-End Trojan Asteroid Rendezvous Tours Incorporating Potential Scientific Value," *AAS/AIAA 24th Space Flight Mechanics Meeting*, Santa Fe, New Mexico, January 26-30 2014. Paper No. AAS-14-267.
- [32] J. R. Stuart, "A Hybrid Systems Strategy for Automated Spacecraft Tour Design and Optimization," Ph.D. Dissertation, School of Aeronautics and Astronautics, Purdue University, West Lafayette, Indiana, 2014.